Hindawi Publishing Corporation
Journal of Nanomaterials
Volume 2015, Article ID 139715, 9 pages
http://dx.doi.org/10.1155/2015/139715

Research Article

Facile Preparation of TiO_2 Nanobranch/Nanoparticle Hybrid Architecture with Enhanced Light Harvesting Properties for Dye-Sensitized Solar Cells

Ju Seong Kim,[1] Seong Sik Shin,[1] Hyun Soo Han,[2] Sun Shin,[1] Jae Ho Suk,[1] Kisuk Kang,[1] Kug Sun Hong,[1] and In Sun Cho[3]

[1]*Research Institute of Advanced Materials, Seoul National University, Seoul 151-744, Republic of Korea*
[2]*Department of Mechanical Engineering, Stanford University, Stanford, CA 94305, USA*
[3]*Department of Materials Science and Engineering and Department of Energy Systems Research, Ajou University, Suwon 443-749, Republic of Korea*

Correspondence should be addressed to Kug Sun Hong; kshongss@plaza.snu.ac.kr and In Sun Cho; cisinsnu@gmail.com

Received 6 January 2015; Accepted 11 March 2015

Academic Editor: Chen Jiangchao

We report TiO_2 nanobranches/nanoparticles (NBN) hybrid architectures that can be synthesized by a facile solution phase method. The hybrid architecture simultaneously improves light harvesting and charge collection performances for a dye-sensitized solar cell. First, TiO_2 nanorods with a trunk length of 2 μm were grown on a fluorine-doped tin oxide (FTO)/glass substrate, and then nanobranches and nanoparticles were deposited on the nanorods' trunks through a solution method using an aqueous $TiCl_3$ solution at 80°C. The relative amount of nanobranches and nanoparticles can be controlled by multiplying the number of $TiCl_3$ treatments to maximize the amount of surface area. We found that the resultant TiO_2 NBN hybrid architecture greatly improves the amount of dye adsorption (five times compared to bare nanorods) due to the enhanced surface area, while maintaining a fast charge collection, leading to a three times higher current density and thus tripling the maximum power conversion efficiency for a dye-sensitized solar cell.

1. Introduction

Dye-sensitized solar cells (DSSCs) have attracted attention as one of the most promising solar conversion devices due to their low fabrication cost and high conversion efficiency [1–4]. In general, a DSSC consists of four parts: the sensitizer (dye molecule), a semiconductor for electron transport, a redox electrolyte, and charge collecting electrodes. Typically, nanoparticle-based photoanodes using n-type semiconductors (TiO_2, ZnO, SnO_2, $BaSnO_3$, Zn_2SnO_4, etc.) have been investigated for adsorption of dye molecules as a result of their large surface areas [4–10]. However, these nanoparticle-based photoanodes limit charge collection efficiency because they have a large number of transport-limiting trapping/detrapping events on the nanoparticle surface; that is, they show a low charge collection efficiency [11, 12].

One strategy for overcoming this low charge collection efficiency is the use of vertically aligned one-dimensional (1D) nanostructures, which offer a direct electron transport pathway to the electrode, thus enabling low charge recombination. To date, various 1D nanostructured photoanodes have been studied, including nanowires (NWs), nanotubes (NTs), nanoparticle-decorated NWs, dendritic NWs, and core/shell NWs [13–19]. For instance, single-crystal TiO_2 nanowires were found to have a large electron diffusion coefficient compared to TiO_2 nanoparticles, owing to a lower density of surface defects [14]. Additionally, a preferentially oriented anatase TiO_2 nanotube, which has a small quantity of high angle grain boundaries, shows a large electron diffusion coefficient and diffusion length compared to TiO_2 nanoparticles [17]. Moreover, dendritic ZnO NWs with multiple branches demonstrated an enhanced photocurrent

and internal quantum efficiency over nanoparticle-based cells [19]. Nevertheless, these 1D nanostructured photoanodes frequently display a low light harvesting efficiency due to a lower dye loading capacity, which leads to a low photocurrent density compared to nanoparticle-based DSSCs [14]. Recently, to address this low dye loading problem in 1D nanostructures, a few studies have adopted hierarchical structures based on the 1D nanostructures (e.g., nanoforests and branched arrays) [20–23]. Even though the hierarchical structures exhibit improved charge collection and light harvesting efficiencies, their preparation methods are somewhat complex and require vacuum equipment, making it difficult to reproduce the synthesis technique and prepare large scale devices.

Here, we report a facile solution phase method to synthesize a TiO_2 nanostructured photoanode consisting of nanobranches/nanoparticles on the trunks of the NWs. These hybrid NWs can be synthesized simply by using an aqueous $TiCl_3$ solution at low temperature (80°C). One advantage of our method is that it enables us to control the relative amount of nanobranches and nanoparticles on the TiO_2 NW trunks as a result of applying multiple $TiCl_3$ treatments, to maximize dye adsorption (i.e., the light harvesting property). Additionally, this method facilitates a scalable preparation (up to a 4-inch wafer) due to it being a low temperature process. We carefully investigated the effect of the $TiCl_3$ treatment on the morphology progress and dye adsorption capacity, and we demonstrate that the hybrid architecture improves the photocurrent and incident photon-to-current conversion efficiency (IPCE) for DSSCs by a factor of two compared to nanorod-based DSSCs.

2. Experimental

2.1. Preparation of the TiO_2 Nanowires (NWs). Rutile TiO_2 NWs were synthesized on a fluorine-doped tin oxide (FTO)/glass substrate by a hydrothermal method [24]. Before growing the TiO_2 nanorods, a TiO_2 seed layer was deposited by a spin coating method using a TiO_2 polymeric sol [25] and then annealed at 450°C for 1 h. Titanium butoxide (97%, Aldrich) was slowly added to 50 mL of a hydrochloric acid (HCl) aqueous solution (25 mL of deionized (DI) water + 25 mL concentrated HCl solution (38%)) and stirred for 30 min to obtain a transparent solution. This precursor solution was transferred into a sealed Teflon-lined stainless steel autoclave (100 mL volume) and then the TiO_2 seed layer-coated FTO/glass substrates were immersed in this solution. The autoclave was placed in an electric oven and heated to 170°C for 6 h without stirring. The resultant TiO_2 nanorod samples were washed with DI water several times and finally annealed at 450°C for 1 h in air.

2.2. $TiCl_3$ Treatment. To grow the nanobranches and nanoparticles, the TiO_2 nanorod samples were immersed into a solution containing 10 mL of DI water, 0.1 mL of concentrated HCl solution, and 1 mL of $TiCl_3$ solution (Aldrich, 10 wt.% in 20–30 wt.% HCl solution) and held at 80°C for 30 min in an oven. The effect of the $TiCl_3$ treatment time (30 min, 1 h, 2 h, and 4 h) on the morphology was examined first. The relative quantity of nanobranches/nanoparticles was controlled by repeating the $TiCl_3$ treatment. We have labeled the sample names as 30 min-1, 30 min-2, 30 min-3, and 30 min-4 to correspond to the number of additional $TiCl_3$ treatments. Afterward, all samples were washed with DI water and annealed at 450°C for 1 h in air.

2.3. Fabrication of DSSCs. The annealed samples were soaked in a ruthenium dye solution (N719, ruthenium (2,2′bipyridyl-4,4′dicarboxylate)$_2$(NCS)$_2$) at room temperature for 12 h. Platinum-coated FTO substrates prepared by sputtering were used as the counter electrodes. The sandwich-type DSSCs were assembled using the samples as the photoanodes and the Pt-coated FTO glasses as the counter electrodes with a hot-melt film (~60 μm, Surlyn, DuPont) as a spacer. Finally, the electrolyte was an iodide-based liquid electrolyte (SI16 L1535-01, Merck), which was introduced into the cell through a hole in the counter electrode. The active area of all samples was 0.25 cm^2.

2.4. Material and DSSC Characterization. The crystal structure and phase of the synthesized samples were identified by an X-ray diffractometer (XRD, Bruker, New D8 Advance) with CuKα radiation operated at 40 kV and 40 mA. The morphologies of the prepared samples were observed by a field-emission scanning electron microscope (FESEM, Hitachi, SU70) and a high-resolution transmission electron microscope (HRTEM, JEOL, JEM-3000F). The photovoltaic performance and electron impedance spectroscopy (EIS) of the DSSCs were measured with a potentiostat (CH Instruments, CHI308C) under AM 1.5G simulated solar light (100 mW/cm^2, Sol3A, Newport). The ultraviolet-visible (UV-Vis) absorption spectra of the dye solutions, collected by desorption from the samples, were investigated with an UV-Vis spectrometer (Agilent Technologies, Cary 5000). The DSSCs' electron transport properties were characterized by intensity-modulated photovoltage spectroscopy (IMVS) using an electrochemical workstation (Zennium, Zahner) with an attached frequency analyzer and a light-emitting diode (667 nm).

3. Results and Discussion

The morphology of the TiO_2 nanorods (NRs) used as the stem for the TiO_2 hybrid architecture is shown in Figures S1 and S2 (in Supplementary Material available online at http://dx.doi.org/10.1155/2015/139715). The NRs are grown on the FTO/glass substrate by a hydrothermal method [26]. The NRs have an average diameter of the length of 103±15 nm and 2.0 ± 0.2 μm (Tables S1 and S2), presenting high crystallinity with a preferred growth direction of [001]. Figure 1 shows top-view FESEM images of the TiO_2 hybrid architectures' microscopic morphologies, prepared by repeating the $TiCl_3$ treatment (1–4 times) at 80°C for 30 min. It can be seen that the $TiCl_3$ treatment significantly affects the morphology of the TiO_2 NRs. After the first $TiCl_3$ treatment (sample 30 min-1), small nanobranches (~10 nm in diameter and

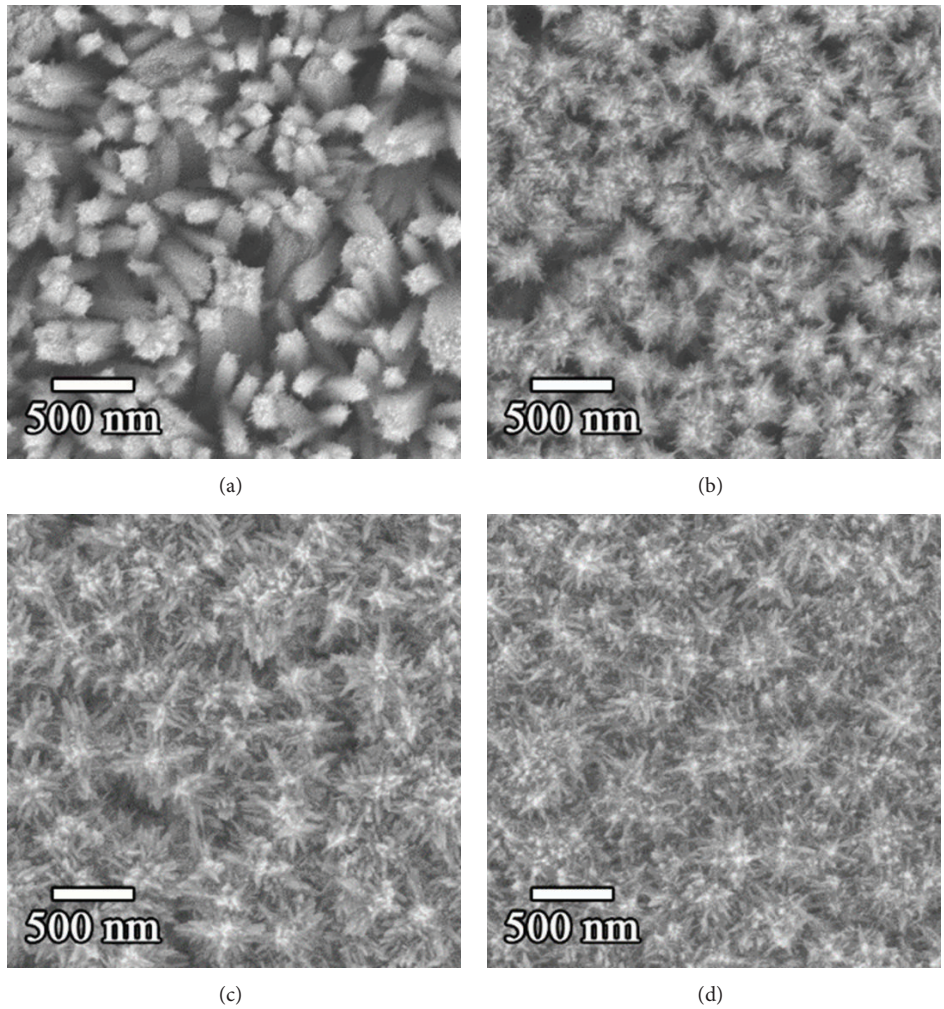

(a) (b)

(c) (d)

Figure 1: The effect of the number of $TiCl_3$ treatments on the morphology of the TiO_2 NWs. Top-view FESEM images, (a) one 30 min treatment (30 min-1), (b) two-time treatments (30 min-2), (c) three-time treatments (30 min-3), and (d) four-time treatments (30 min-4).

~60 nm in length) were formed on the surface of the individual TiO_2 NRs (Figure 1(a)), which lengthen further (~100 nm long) with an increased density on the NR surface after the second $TiCl_3$ treatment (sample 30 min-2, Figure 1(b)). When the treatment was repeated three times (sample 30 min-3, Figure 1(c)), the length of the nanobranches increased to 200–300 nm, reducing the interspaces between the TiO_2 NRs; these interspaces decreased significantly after the fourth treatment (sample 30 min-4, Figure 1(d)). We also investigated the effects of the $TiCl_3$ treatment duration time (Figure S3). An increased duration time provides a similar effect on the morphology; that is, it lengthens the nanobranches and increases their density as the duration time was increased from 30 min to 4 h.

The detailed variation in the TiO_2 nanostructure morphology with multiple $TiCl_3$ treatments was investigated further by utilizing cross-sectional FESEM images (Figure 2). For the 30 min-1 and 30 min-2 samples, there were no significant changes in the TiO_2 NRs except for the formation of nanobranches. However, for the 30 min-3 sample, the nanobranches grew in length, reducing the space between NRs, especially at their tops (Figure 2(c)). Interestingly, at the bottom of the nanorods, nanoparticles with an average size of ~30 nm formed together with the nanobranches, suggesting that more than three $TiCl_3$ treatments induce a different growth mode, generating nanoparticles at the bottom of the NRs. Finally, after the fourth treatment (30 min-4), the TiO_2 nanoparticles completely filled the NR interspaces, up to the top of the film. These two different growth modes, that is, the nanobranch and nanoparticle growth, during the multiple $TiCl_3$ treatments enable the morphology to be tuned, thereby controlling the relative surface area of the 1D nanostructure based on the NRs.

The XRD patterns of the samples discussed above are shown in Figure 3. All diffraction peaks of the TiO_2 NRs (30 min-1) are in agreement with tetragonal rutile TiO_2 (JCPDS number 21-1276, $P4_2/mnm$, $a = b = 4.593$ Å, $c = 2.959$ Å). In general, rutile TiO_2 NRs prepared by a hydrothermal method grow along the (001) plane, as it has the fastest growth rate compared to the other crystal faces [13, 27, 28]. Similar to other reports, our TiO_2 NRs have a preferred growth direction of [001], which was

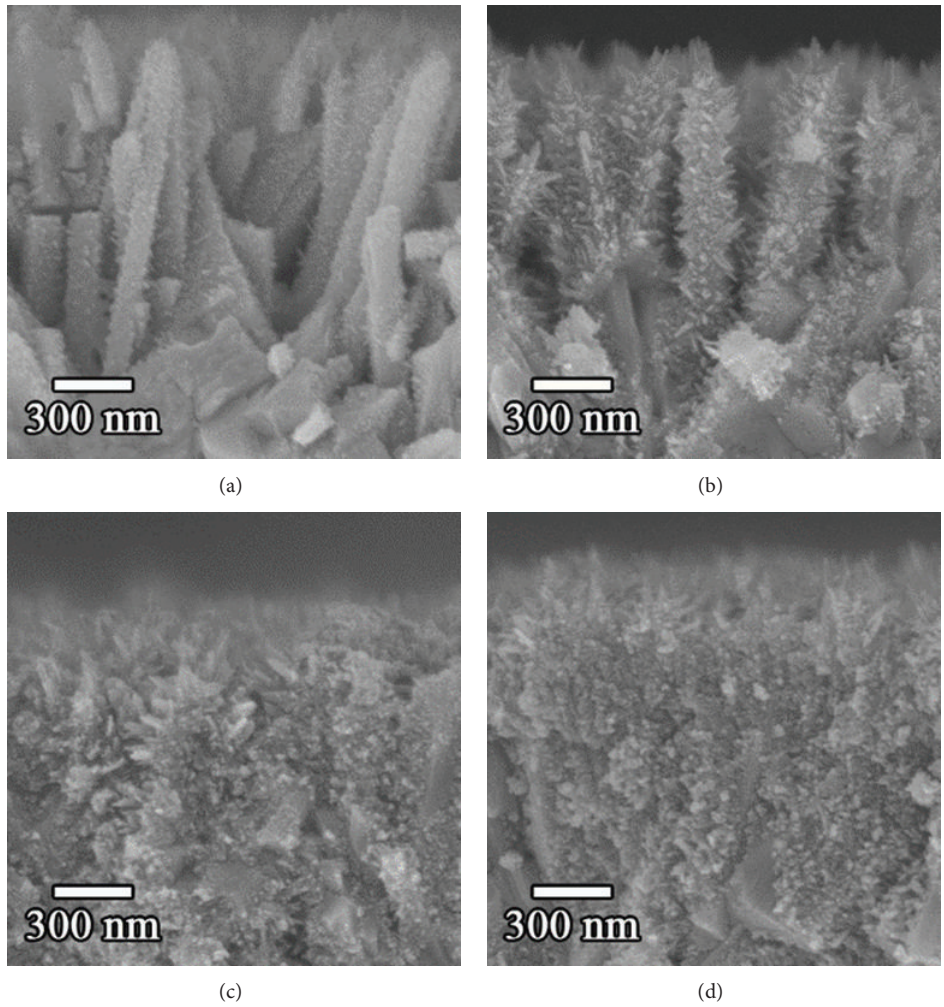

FIGURE 2: Cross-sectional SEM images of the TiO_2 NWs obtained by repeating the $TiCl_3$ treatments, (a) 30 min-1, (b) 30 min-2, (c) 30 min-3, and (d) 30 min-4. After three $TiCl_3$ treatments, nanoparticles start to form and fill the gaps between NWs.

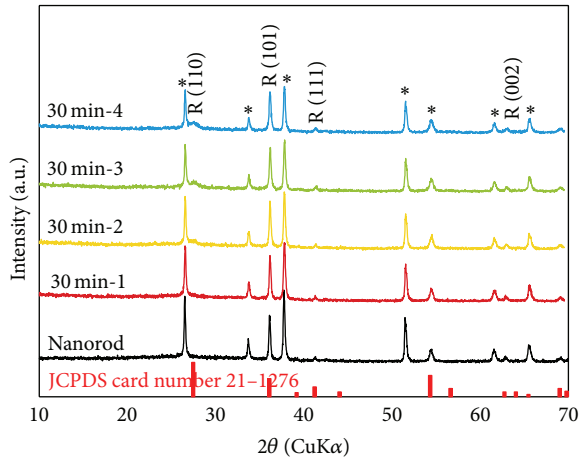

R: rutile TiO_2
*: FTO

FIGURE 3: XRD patterns of TiO_2 NWs and hybrid architectures obtained by the $TiCl_3$ treatments (0–4 times).

also confirmed by a TEM analysis (Figure S2). For the XRD peaks of the multiple $TiCl_3$ treatment samples, there were no considerable differences from the 30 min-1 sample, suggesting that the nanobranches and nanoparticles are also rutile tetragonal structures. The perceptible development of the (110) diffraction peaks at 27.5° in the 30 min-2, 30 min-3, and 30 min-4 samples implies that the nanobranches have the same preferred [001] growth direction [24].

Based on the above observation, the formation process of the TiO_2 nanobranch/nanoparticle (NBN) hybrid architectures is displayed schematically in Figure 4. After the first treatment, short nanobranches are formed on the surface of the NRs, which grow to longer nanobranches with an average length of ~100 nm after the second $TiCl_3$ treatment. The third $TiCl_3$ treatment induces nanoparticle growth from the bottom of the film, which reduces the interspaces between the NRs at their bases. With a further $TiCl_3$ treatment, however, additional nanoparticles formed, filling the remaining interspaces between the NRs to the top of the film, finally forming a NBN hybrid architecture.

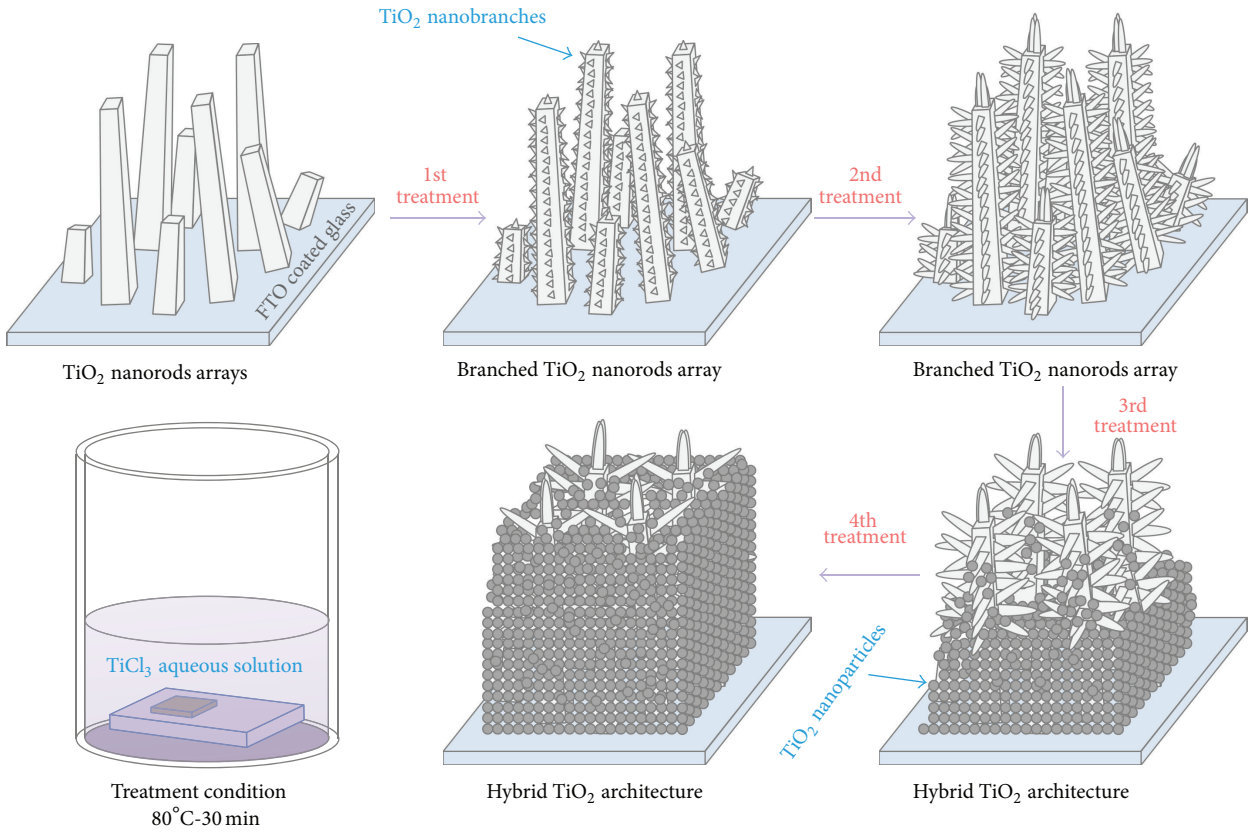

Figure 4: Schematic illustration of the TiO_2 hybrid architecture formation process.

It should be noted that these interesting 1D architectures are obtained by simply repeating the $TiCl_3$ treatment, which enabled the unusual growth (or deposition) behavior during the additional $TiCl_3$ treatments. In general, the pH of the growth solution significantly affects the growth morphology (i.e., the crystal phase and morphology) of TiO_2 nanocrystals [29], that is, nanoparticles near pH 7 and elongated nanorods or nanoneedles below pH 4. Therefore, the two different growth modes, of the nanobranches and nanoparticles, might relate to the change in the solution's pH value during the multiple $TiCl_3$ treatments. A detailed analysis of this is under investigation.

Next, in order to check the usefulness of the NBN hybrid architectures for a solar energy conversion device, we fabricated dye-sensitized solar cells (DSSCs) with them. First, the light harvesting behavior, that is, the dye adsorption property, was investigated by UV/Vis absorption spectroscopy (Figure 5). The absorption spectra were obtained of dye solutions after collecting the dye by a desorption process in a basic solution. The peak at 510 nm in the absorption spectra is a characteristic peak of these dye molecules (N719), and this can be used to estimate the amount of dye molecules adsorbed onto the TiO_2 surface. As shown in the inset of Figure 5, the amount of adsorbed dye molecules continued to increase with repeated $TiCl_3$ treatments, before becoming saturated with the 30 min-3 sample. The amount of adsorbed dye of the 30 min-4 sample increased nearly by a factor of four compared to the 30 min-0 sample, indicating that the NBN hybrid architecture (30 min-4 sample) has a larger surface area, thus improving the light harvesting efficiency for the DSSCs.

Figure 6(a) shows the photocurrent density-voltage curves of the DSSCs fabricated using the above four samples, which were measured under AM 1.5G simulated solar light (1 sun, 100 mW/cm^2) and their representative solar cell parameters are shown in Figures 6(b) and 6(c) (with the other parameters summarized in Table 1). Initially, the short circuit photocurrent density (J_{sc}) values increased linearly until the third treatment and eventually reaching a maximum J_{sc} value of 13.4 mA/cm^2 for the fourth treatment. This result strongly correlates with the absorbance spectra of the desorbed dye shown in the inset of Figure 5, indicating that the NBN hybrid architecture has an improved light harvesting property, thus increasing the J_{sc} for DSSCs. The open circuit voltage (V_{oc}) of the TiO_2 NR-based DSSC was 0.82 V. This V_{oc} value decreased slightly with an increasing number of $TiCl_3$ treatments to 0.77, 0.72, 0.71, and 0.69 V for the 30 min-1, 30 min-2, 30 min-3, and 30 min-4 samples, respectively. In the case of the fill factor (FF) values, there were no notable differences (Table 1). As a result, the power conversion efficiency was enhanced from 2.6% (for the NR-based DSSC) to

Table 1: The photocurrent density-voltage characteristics and dye loading of the NBN-TiO_2-based DSSCs with various $TiCl_3$ treatment times.

Photoelectrode	J_{sc} [mA/cm^2]	V_{oc} [V]	FF [%]	η [%]	Dye loading [$\times 10^{-9}$ mole/cm^3]
Nanorod	5.62	0.82	57	2.6	0.34
30 min-1	7.86	0.77	58	3.5	0.43
30 min-2	11.26	0.72	58	4.7	0.92
30 min-3	12.95	0.71	57	5.2	1.50
30 min-4	13.35	0.69	58	5.3	1.65

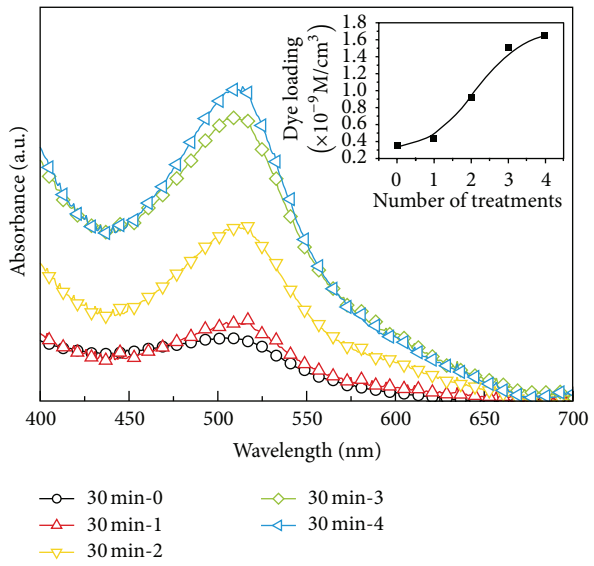

Figure 5: The UV-Vis absorption spectra of the dye (N719) detached from the TiO_2 films prepared under a varied number of $TiCl_3$ treatments. To measure the UV-Vis absorption spectra of the dye (N719), it was first desorbed by an ammonium (NH_4OH) solution in water and ethanol (50 : 50, v/v).

5.3% (for the NBN hybrid architecture- (30 min-4-) based DSSC), demonstrating that the NBN hybrid architecture is advantageous to improve J_{sc} in DSSCs.

To understand the effect of the multiple $TiCl_3$ treatments on the electron dynamics, an intensity-modulated photocurrent/photovoltage spectroscopy (IMPS/IMVS) was used to measure the samples (Figure S4). All samples show a typical power-law dependence of their transport time constants on the J_{sc} value (Figure S4a). This indicates an exclusive random walk of photoelectrons between trap sites having a power-law distribution of waiting (release) times in the form of $\tau^{-1-\alpha}$, where the parameter α can be related to the shape of the trap distribution [30, 31]. Initially, the charge transport time increased with the additional $TiCl_3$ treatments, indicating that the route photoelectrons travel to the FTO substrate became longer and more complicated due to the nanobranches and nanoparticles. This reduction in the transport time constant competes with the effect of the increased dye adsorption. The transport time constant and the dye adsorption correlate to the charge collection efficiency and light harvesting efficiency, respectively, which determine the power conversion efficiency. However, since the effects of the dye adsorption are dominant, the power conversion efficiency of the TiO_2 NBN hybrid architecture DSSC increased with repeated $TiCl_3$ treatments.

Second, the charge recombination time constant consistently decreased with an increasing number of $TiCl_3$ treatments. The infiltrated TiO_2 nanobranches and nanoparticles decreased the diffusion efficiency of the I_3^- ions in the electrolyte. The relation between the recombination time and V_{oc} can be described by the following equation [32, 33]:

$$V_{oc} = \frac{RT}{\beta F} \ln\left(\frac{AI}{n_0 k_1 [I_3^-] + n_0 k_2 [D^+]}\right), \quad (1)$$

where R is the molar gas constant, T is the temperature, β is the reaction order for the electrons, F is the Faraday constant, A is the electrode area, I is the incident photon flux, n_0 is the concentration of accessible electronic states in the conduction band, and k_1 and k_2 are the kinetic constants of the injected electron with triiodide (I_3^-) back reaction and the recombination of these electrons with oxidized dye (D^+) molecules, respectively. Neglecting the recombination of the injected electrons with oxidized dye molecules, the V_{oc} value is logarithmically dependent on the back reaction of these electrons with the triiodide (k_1). Therefore, the rate of the electron recombination from the TiO_2 photoanode to the I_3^- ions in the electrolyte increased with an increasing number of $TiCl_3$ treatments.

Figure 7 shows the incident photon-to-current efficiency (IPCE) spectra of the TiO_2 photoanode-based DSSCs. All of the DSSCs show the typical spectral response of N719-based DSSCs with a peak at approximately 530 nm. However, the maximum IPCE (or external quantum efficiency, EQE) varies with the number of $TiCl_3$ treatments. The 30 min-4 sample exhibited the maximum IPCE and the NR sample displayed the minimum IPCE. The IPCE of DSSCs is determined by the light harvesting efficiency (η_{lh}), the charge injection efficiency (η_{inj}), and the charge collection efficiency (η_{cc}). The IPCE value can be expressed by the following equation:

$$\text{IPCE}\,(\%) = \eta_{lh} \times \eta_{inj} \times \eta_{cc}. \quad (2)$$

The light harvesting efficiency is generally affected by the dye loading capacity [34]. As mentioned in Figure 5, the dye loading capacity of the TiO_2 photoanodes increased significantly with multiple $TiCl_3$ treatments, implying that the light harvesting efficiency increased with additional $TiCl_3$ treatments. On the other hand, the IMPS and IMVS data (Figure S4) demonstrate that the charge collection efficiency decreased monotonically with the multiple $TiCl_3$ treatments.

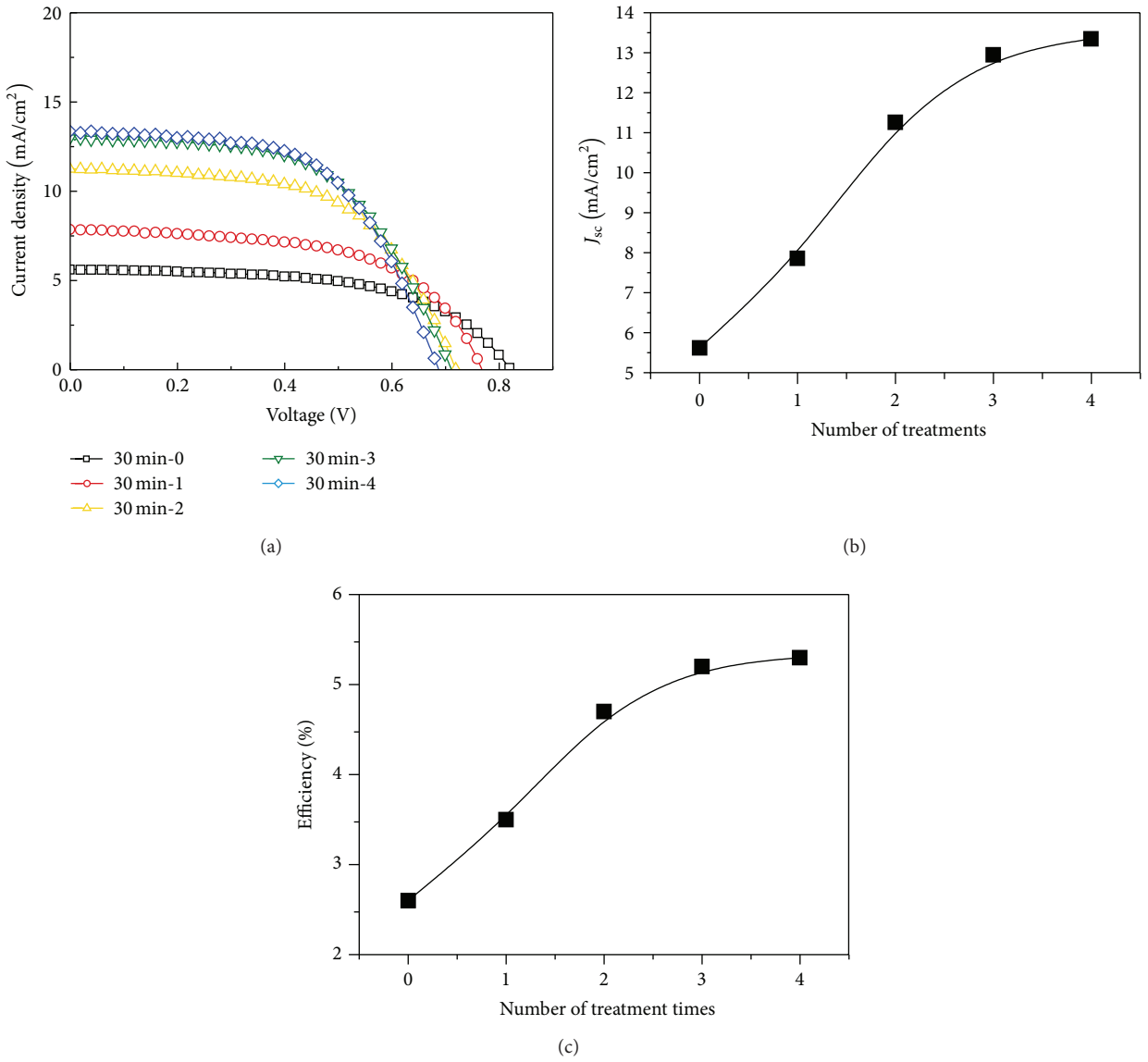

FIGURE 6: (a) The photocurrent density-voltage curves of the NBN-TiO_2-based DSSCs measured under AM 1.5G, at a 1 sun light intensity, using a shadow mask. Effect of treatment times on (b) photocurrent density (J_{sc}) and (c) efficiency (%).

Even though the NBN hybrid architecture reduced the electron transport property slightly, it can be concluded that the enhancement seen in the light harvesting efficiency was greater than the decrease in the charge collection efficiency. Interestingly, the IPCE values of the samples after multiple $TiCl_3$ treatments show a shoulder at a longer wavelength (>680 nm), indicating that the NBN hybrid architecture has additional enhancement effects for DSSCs, that is, improving the light scattering effect. This light scattering effect also enhances the light harvesting efficiency in combination with the increased dye loading capacity.

4. Conclusions

In summary, we report on a TiO_2 hybrid architecture composed of TiO_2 nanobranches and nanoparticles, easily synthesized by a solution phase method. A $TiCl_3$ aqueous solution treatment at 80°C enables a controlled morphology of the TiO_2 nanorods. By repeating this $TiCl_3$ treatment, nanobranches and/or nanoparticles are deposited on the trunks of the TiO_2 nanorods, giving hybrid architecture with an enhanced surface area. We found that the resultant TiO_2 nanobranch/nanoparticle hybrid architecture greatly improved the dye adsorption (five times compared to bare nanorods) due to the enhanced surface area, albeit a slight decrease in a charge collection property. Additionally, the complex architecture produces a large light scattering effect, eventually leading to a three times greater current density and thus tripling the maximum power conversion efficiency for a dye-sensitized solar cell. We believe that the synthesized TiO_2 hybrid architecture, after further structural optimization, has the potential for use in other energy harvesting devices

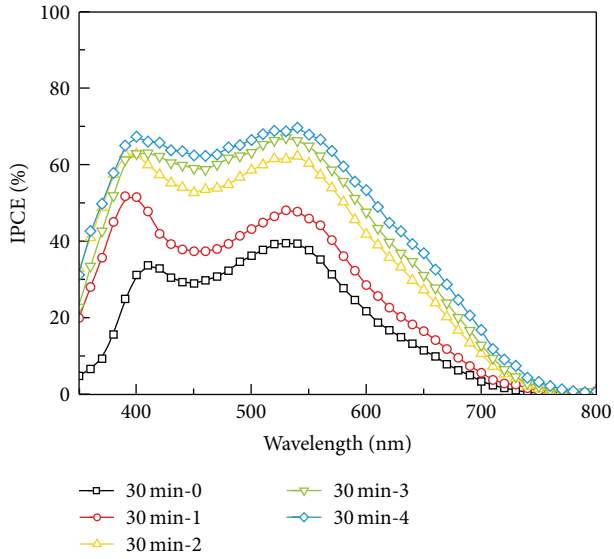

FIGURE 7: The incident photon-to-current conversion efficiency (IPCE) spectra of the TiO_2 hybrid architecture-based DSSCs with various $TiCl_3$ treatment times.

such as quantum-dot dye-sensitized solar cells (QD-DSSCs), photoelectrochemical (PEC) water-splitting, and solid-state solar cells, which require both high light harvesting and charge collection efficiencies.

Conflict of Interests

The authors declare that there is no conflict of interests regarding the publication of this paper.

Acknowledgment

This work was partially supported by the new faculty research fund of Ajou University (S-2014-G0001-00309).

References

[1] M. Grätzel, "Dye-sensitized solar cells," *Journal of Photochemistry and Photobiology C: Photochemistry Reviews*, vol. 4, no. 2, pp. 145–153, 2003.

[2] B. O'Regan and M. Graetzel, "A low-cost, high-efficiency solar cell based on dye-sensitized colloidal TiO_2 films," *Nature*, vol. 353, no. 6346, pp. 737–740, 1991.

[3] M. Grätzel, "Solar energy conversion by dye-sensitized photovoltaic cells," *Inorganic Chemistry*, vol. 44, no. 20, pp. 6841–6851, 2005.

[4] A. Yella, H.-W. Lee, H. N. Tsao et al., "Porphyrin-sensitized solar cells with cobalt (II/III)-based redox electrolyte exceed 12 percent efficiency," *Science*, vol. 334, no. 6056, pp. 629–634, 2011.

[5] T. P. Chou, Q. Zhang, G. E. Fryxell, and G. Cao, "Hierarchically structured ZnO film for dye-sensitized solar cells with enhanced energy conversion efficiency," *Advanced Materials*, vol. 19, no. 18, pp. 2588–2592, 2007.

[6] Q. Zhang, T. P. Chou, B. Russo, S. A. Jenekhe, and G. Cao, "Aggregation of ZnO nanocrystallites for high conversion efficiency in dye-sensitized solar cells," *Angewandte Chemie*, vol. 120, no. 13, pp. 2436–2440, 2008.

[7] J. Liu, T. Luo, S. Mouli T, F. Meng, B. Sun, and M. Li, "A novel coral-like porous SnO_2 hollow architecture: biomimetic swallowing growth mechanism and enhanced photovoltaic property for dye-sensitized solar cell application," *Chemical Communications*, vol. 46, no. 3, pp. 472–474, 2010.

[8] A. Kay and M. Grätzel, "Dye-sensitized core-shell nanocrystals: Improved efficiency of mesoporous tin oxide electrodes coated with a thin layer of an insulating oxide," *Chemistry of Materials*, vol. 14, no. 7, pp. 2930–2935, 2002.

[9] S. S. Shin, J. S. Kim, J. H. Suk et al., "Improved quantum efficiency of highly efficient perovskite $BaSnO_3$-based dye-sensitized solar cells," *ACS Nano*, vol. 7, no. 2, pp. 1027–1035, 2013.

[10] D. W. Kim, S. S. Shin, I. S. Cho et al., "Synthesis and photovoltaic property of fine and uniform Zn_2SnO_4 nanoparticles," *Nanoscale*, vol. 4, no. 2, pp. 557–562, 2012.

[11] J. H. Noh, H. S. Han, S. Lee et al., "Nanowire-based three-dimensional transparent conducting oxide electrodes for extremely fast charge collection," *Advanced Energy Materials*, vol. 1, no. 5, pp. 829–835, 2011.

[12] W.-Q. Wu, J.-Y. Liao, H.-Y. Chen, X.-Y. Yu, C.-Y. Su, and D.-B. Kuang, "Dye-sensitized solar cells based on a double layered TiO_2 photoanode consisting of hierarchical nanowire arrays and nanoparticles with greatly improved photovoltaic performance," *Journal of Materials Chemistry*, vol. 22, no. 34, pp. 18057–18062, 2012.

[13] B. Liu and E. S. Aydil, "Growth of oriented single-crystalline rutile TiO_2 nanorods on transparent conducting substrates for dye-sensitized solar cells," *Journal of the American Chemical Society*, vol. 131, no. 11, pp. 3985–3990, 2009.

[14] X. Feng, K. Zhu, A. J. Frank, C. A. Grimes, and T. E. Mallouk, "Rapid charge transport in dye-sensitized solar cells made from vertically aligned single-crystal rutile TiO_2 nanowires," *Angewandte Chemie International Edition*, vol. 51, no. 11, pp. 2727–2730, 2012.

[15] G. K. Mor, K. Shankar, M. Paulose, O. K. Varghese, and C. A. Grimes, "Use of highly-ordered TiO_2 nanotube arrays in dye-sensitized solar cells," *Nano Letters*, vol. 6, no. 2, pp. 215–218, 2006.

[16] J. R. Jennings, A. Ghicov, L. M. Peter, P. Schmuki, and A. B. Walker, "Dye-sensitized solar cells based on oriented TiO_2 nanotube arrays: transport, trapping, and transfer of electrons," *Journal of the American Chemical Society*, vol. 130, no. 40, pp. 13364–13372, 2008.

[17] S. Lee, I. J. Park, D. H. Kim et al., "Crystallographically preferred oriented TiO_2 nanotube arrays for efficient photovoltaic energy conversion," *Energy and Environmental Science*, vol. 5, no. 7, pp. 7989–7995, 2012.

[18] M. Law, L. E. Greene, J. C. Johnson, R. Saykally, and P. Yang, "Nanowire dye-sensitized solar cells," *Nature Materials*, vol. 4, no. 6, pp. 455–459, 2005.

[19] Y. Gao, M. Nagai, T.-C. Chang, and J.-J. Shyue, "Solution-derived ZnO nanowire array film as photoelectrode in dye-sensitized solar cells," *Crystal Growth and Design*, vol. 7, no. 12, pp. 2467–2471, 2007.

[20] S. H. Ko, D. Lee, H. W. Kang et al., "Nanoforest of hydrothermally grown hierarchical ZnO nanowires for a high efficiency

dye-sensitized solar cell," *Nano Letters*, vol. 11, no. 2, pp. 666–671, 2011.

[21] H. Wang, Y. Bai, Q. Wu et al., "Rutile TiO_2 nano-branched arrays on FTO for dye-sensitized solar cells," *Physical Chemistry Chemical Physics*, vol. 13, no. 15, pp. 7008–7013, 2011.

[22] W.-P. Liao and J.-J. Wu, "Wet chemical route to hierarchical TiO_2 nanodendrite/ nanoparticle composite anodes for dye-sensitized solar cells," *Journal of Materials Chemistry*, vol. 21, no. 25, pp. 9255–9262, 2011.

[23] F. Shao, J. Sun, L. Gao, S. Yang, and J. Luo, "Forest-like TiO_2 hierarchical structures for efficient dye-sensitized solar cells," *Journal of Materials Chemistry*, vol. 22, no. 14, pp. 6824–6830, 2012.

[24] I. S. Cho, Z. Chen, A. J. Forman et al., "Branched TiO_2 nanorods for photoelectrochemical hydrogen production," *Nano Letters*, vol. 11, no. 11, pp. 4978–4984, 2011.

[25] H. S. Jung, J.-K. Lee, B. S. Kang, Q. Jia, and M. Nastasi, "Strain relaxation in sol-gel grown epitaxial anatase thin films," *The Journal of Physical Chemistry C*, vol. 112, no. 11, pp. 4205–4208, 2008.

[26] E. Hosono, S. Fujihara, K. Kakiuchi, and H. Imai, "Growth of submicrometer-scale rectangular parallelepiped rutile TiO_2 films in aqueous $TiCl_3$ solutions under hydrothermal conditions," *Journal of the American Chemical Society*, vol. 126, no. 25, pp. 7790–7791, 2004.

[27] H. Cheng, J. Ma, Z. Zhao, and L. Qi, "Hydrothermal preparation of uniform nanosize rutile and anatase particles," *Chemistry of Materials*, vol. 7, no. 4, pp. 663–671, 1995.

[28] H. Perron, C. Domain, J. Roques, R. Drot, E. Simoni, and H. Catalette, "Optimisation of accurate rutile TiO_2 (110), (100), (101) and (001) surface models from periodic DFT calculations," *Theoretical Chemistry Accounts*, vol. 117, no. 4, pp. 565–574, 2007.

[29] S. Lee, I.-S. Cho, J. H. Lee et al., "Two-step sol-gel method-based TiO_2 nanoparticles with uniform morphology and size for efficient photo-energy conversion devices," *Chemistry of Materials*, vol. 22, no. 6, pp. 1958–1965, 2010.

[30] J. Nelson, S. A. Hague, D. R. Klug, and J. R. Durrant, "Trap-limited recombination in dye-sensitized nanocrystalline metal oxide electrodes," *Physical Review B*, vol. 63, no. 20, Article ID 205321, 9 pages, 2001.

[31] J. van de Lagemaat and A. J. Frank, "Nonthermalized electron transport in dye-sensitized nanocrystalline TiO_2 films: transient photocurrent and random-walk modeling studies," *The Journal of Physical Chemistry B*, vol. 105, no. 45, pp. 11194–11205, 2001.

[32] Q. Wang, J.-E. Moser, and M. Grätzel, "Electrochemical impedance spectroscopic analysis of dye-sensitized solar cells," *The Journal of Physical Chemistry B*, vol. 109, no. 31, pp. 14945–14953, 2005.

[33] D. Hwang, D. Y. Kim, and S. Y. Jang, "Superior photoelectrodes for solid-state dye-sensitized solar cells using amphiphilic TiO_2," *Journal of Materials Chemistry A*, vol. 1, no. 4, pp. 1228–1238, 2013.

[34] J.-H. Yum, S.-R. Jang, R. Humphry-Baker et al., "Effect of coadsorbent on the photovoltaic performance of zinc pthalocyanine-sensitized solar cells," *Langmuir*, vol. 24, no. 10, pp. 5636–5640, 2008.